A.Y. VOROBYEV
CHUNLEI GUO[✉]

Shot-to-shot correlation of residual energy and optical absorptance in femtosecond laser ablation

The Institute of Optics, University of Rochester, Rochester, NY 14627, USA

ABSTRACT In this paper, we perform a shot-to-shot detailed study of how residual thermal energy correlates to the optical absorptance change due to laser-induced surface structural modifications in multi-shot femtosecond laser ablation. We observe an overall enhancement for residual thermal coupling and absorptance in air. Surprisingly, residual thermal coupling in air shows a non-monotonic dependence on pulse number and reaches a minimum value after a certain number of pulses, while these behaviors are not seen in absorptance. In vacuum, however, both suppression and enhancement are seen in residual energy coupling although absorptance is always enhanced. To explain these observations, we suggest that air plasma plays a dominant role in thermal coupling at a relatively low number of applied pulses, while the formation of a cavity plays a dominant role at a high number of pulses.

PACS 78.20.Ci; 81.05.Bx

1   Introduction

Femtosecond laser ablation [1] has been demonstrated to be a promising technique for various applications in nanotechnology [2–5], high-precision materials machining [6, 7], and thin film-deposition [8]. However, the physical mechanisms of femtosecond laser ablation are still not fully understood. For example, recent studies have shown that the residual thermal energy in an ablated metal sample abruptly increases following both single-pulse and pulse-train femtosecond laser ablation in a gas medium when the laser fluence is above a certain threshold [9, 10]. In the case of pulse-train ablation [10], it was found that one contributing factor to the enhanced thermal coupling following a large number of applied pulses is the increased sample absorptance due to surface structural modifications. However, we have shown that the surface modifications alone cannot fully explain the enhanced thermal energy deposition [10]. To further study the effects of the enhanced thermal coupling to metals, in this paper we perform a shot-to-shot detailed study of how residual energy correlates to the absorptance change due to surface structural modifications. We observe an overall enhancement

[✉] Fax: +1-585-244-4936, E-mail: guo@optics.rochester.edu

for residual thermal coupling and absorptance in air. Surprisingly, residual thermal coupling in air shows a non-monotonic dependence on pulse number and reaches a minimum value after a certain number of pulses, while these behaviors are not seen in absorptance. In vacuum, however, both suppression and enhancement are seen in residual energy coupling although absorptance is always enhanced. To explain these observations, we suggest that air plasma plays a dominant role in thermal coupling at a relatively low number of applied pulses, while the formation of a cavity plays a dominant role at a high number of pulses.

2   Experimental setup

The laser used in the experiment is an amplified Ti:sapphire system generating 65-fs pulses of about 1.5 mJ/pulse at a 1-kHz repetition rate with the central wavelength at 800 nm. Our experimental setup is shown in Fig. 1. To produce ablation, the laser beam is focused onto a platinum (Pt) bulk sample at normal incidence. The Pt sample is mechanically polished before experiments. The number of laser pulses, N, delivered to the sample is controlled by a fast electromechanical shutter.

In the ablation, some directly absorbed laser energy will be carried away by the ablated material, while a fraction of the absorbed pulse energy will remain in the surface layer of the sample, dissipate into the bulk sample due to heat conduction, and remain in the sample as residual thermal energy. The remaining energy following ablation will cause the bulk sample temperature to rise. Furthermore, there can be indirect mechanisms contributing to the residual heating of the sample, such as re-deposition of the hot ablated material back onto the sample and exothermic chemical reactions. To characterize the total residual thermal energy coupling to the sample, we define a residual energy coefficient (REC), K, as $K = E_R/E_I$, where E_R is the total residual energy remaining in the sample following ablation and E_I is the pulse energy incident onto the sample. To measure E_R, we apply a calorimetric technique that has been described in our previous studies [9, 10]. Briefly, we measure the bulk temperature rise ΔT_R with a thermocouple battery following ablation and determine E_R calorimetrically as $E_R = mC\Delta T_R$, where m is the mass and C is the known specific heat capacity of the sample. The measurement uncertainty for E_R is estimated to be about 10%. To measure
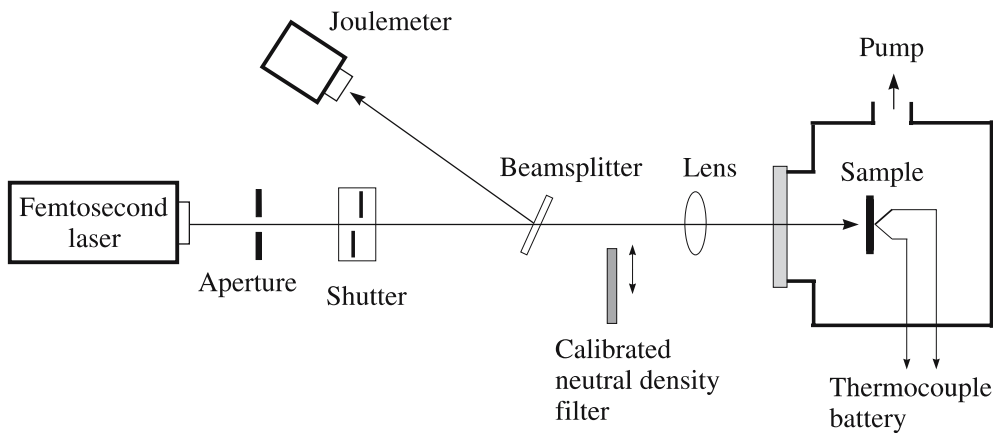
E_I, a fraction of the incident pulse energy is split off by a beam splitter and diverted to a pyroelectric joule meter. The measurement uncertainty for E_I is estimated to be about 5%. This calorimetric technique can also be used to study the change of the sample absorptance due to laser-induced surface modifications by applying the following procedure that has also been described in our previous work [11]. To determine the absorptance of a damaged material following pulse ablation, we attenuate the laser fluence with a neutral density filter to a level much below the ablation threshold and apply the same calorimetric technique as used in determining REC. Briefly, after ablation we will irradiate the ablated spot using a train of low-fluence laser pulses that will not produce any further surface modifications. The absorbed fraction of this low-fluence pulse train energy, E_A, will dissipate into the sample due to heat conduction and cause the bulk temperature of the whole sample to rise by ΔT_A. We measure ΔT_A with the thermocouple battery and determine calorimetrically the energy E_A absorbed by the sample. Having also measured the total energy of the low-fluence pulse train, E_{IT}, the absorptance of the sample following laser ablation is determined as $A = E_A/E_{IT}$. Thus, our calorimetric technique allows us to measure both REC and absorptance of the ablated sample and to determine the relationship between REC and absorptance. Our experimental procedure is as follows. We apply the first laser pulse to an undamaged Pt sample with fluence above the ablation threshold and determine REC. We then attenuate the beam with the neutral density filter and measure the absorptance of the ablated spot. Next, we remove the filter, apply the second high-fluence pulse, and determine REC; we then re-insert the filter and measure the absorptance A following two-pulse ablation. This measurement is repeated at the same sample spot, so we can determine both REC and A as a function of pulse number N. Our experiment is carried out both in 1-atm air and in a vacuum at a base pressure of 6×10^{-3} Torr. The number of applied laser shots is varied from 1 to 1000. Following ablation, the ablated spots are examined under a scanning electron microscope (SEM).

3   Experimental results

Following femtosecond laser ablation, the residual energy coefficient $K(N)$ and low-fluence absorptance $A(N)$ are studied as functions of the number of applied laser pulses,

N, at single-pulse laser fluences of $F = 9.0$ and $3.6\,\text{J/cm}^2$ in both air and vacuum. The single-pulse ablation threshold F_{abl} for the mechanically polished Pt surface is determined to be $F_{abl} = 0.15\,\text{J/cm}^2$. The number of pulses required to drill through a 0.25-mm-thick Pt sample in air is determined to be 920 and 1530 at $F = 9.0$ and $3.6\,\text{J/cm}^2$, respectively. This gives an average ablation rate of 272 and 163 nm/pulse for the two fluence levels. As a reference, we also measure the low-fluence absorptance $A_0(N)$ for an undamaged surface at a fluence much below the ablation threshold. This $A_0(N)$ is shown with the cross symbols in Fig. 2. One can see that A_0 has a constant value of about 0.34 and is independent of the number of applied shots, indicating that this laser fluence is indeed low enough and no heat accumulation effects are involved. This value of A_0 (~ 0.34) agrees with the table value of the absorptance for mechanically polished Pt at $\lambda = 800$ nm [12]. The dependences of REC and absorptance on the number of ablation shots at $F = 9.0\,\text{J/cm}^2$ in 1-atm air are shown in Fig. 2. We notice two distinct regions in the behaviors of $K(N)$ and $A(N)$. For $N < 12$, REC decreases with N while, for $N > 12$, REC increases with N. An important feature in the behavior of REC is that the highest REC value ($K = 0.76$) is reached by only one single-pulse ablation although the absorptance of the undamaged surface before the first pulse ablation is the
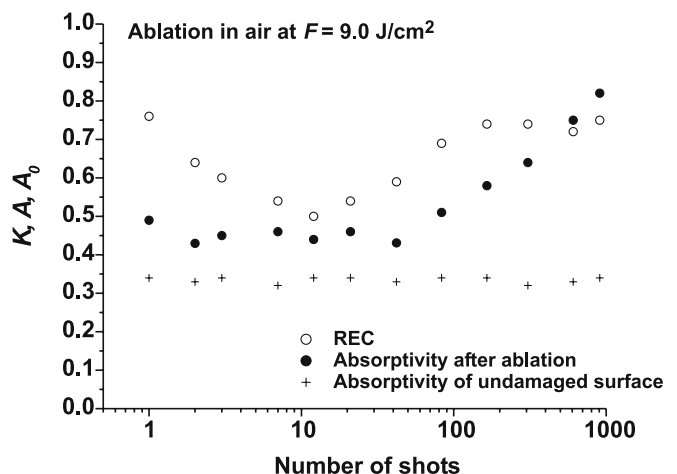
lowest ($A = 0.34$). Following the second pulse ablation, REC decreases from 0.76 to 0.64 although the sample absorptance ($A = 0.5$) before the second pulse is much higher than the undamaged surface value. For $2 < N < 12$, REC decreases while the absorptance remains virtually the same. These data clearly show that for low N the enhanced absorptance compared to the undamaged surface is not the dominant factor for the enhanced residual thermal heating. For $N > 20$, REC starts to increase with N and reaches a saturation level of about 0.75 at $N \approx 200$. Therefore, in the range of N studied in this experiment, about 50%–75% of the incident pulse energy remains in the sample as residual thermal energy (thermal load). The $A(N)$ data in Fig. 2 show that the absorptance enhances from 0.34 (undamaged surface) to 0.5 following single-pulse ablation and then remains approximately constant for $N < 30$. To determine the surface structures associated with the absorptance enhancement, we take SEM images of the sample surface. As shown in Fig. 3, the enhanced surface absorptance mainly results from the laser-induced micro- and nanorough-

ness [11]. (We note that microstructures on semiconductors have been produced using femtosecond laser-assisted chemical etching, and these microstructures can also lead to an enhanced optical absorptance [13].) On further increasing N, we observe the formation of an ablation-induced cavity (see Fig. 4a) and both REC and absorptance increase as the cavity develops. From Fig. 2, we can see that A surpasses K when $N > 600$.

The behaviors of $A_0(N)$, $A(N)$, and $K(N)$ measured in a vacuum are shown in Fig. 5. We can see that the low-fluence absorptance $A_0(N)$ of an undamaged surface is about the same as the value measured in air. The overall behavior of $A(N)$ in vacuum is similar to that in air, although the absorptance enhancement due to surface structural modifications is greater in vacuum compared to that in air. However, the dependence of K on N in vacuum is very different from that in air. We can see that following the first pulse ablation, REC reaches a value of 0.15 in vacuum, well below the value of absorptance of the undamaged surface. This low REC value in vacuum
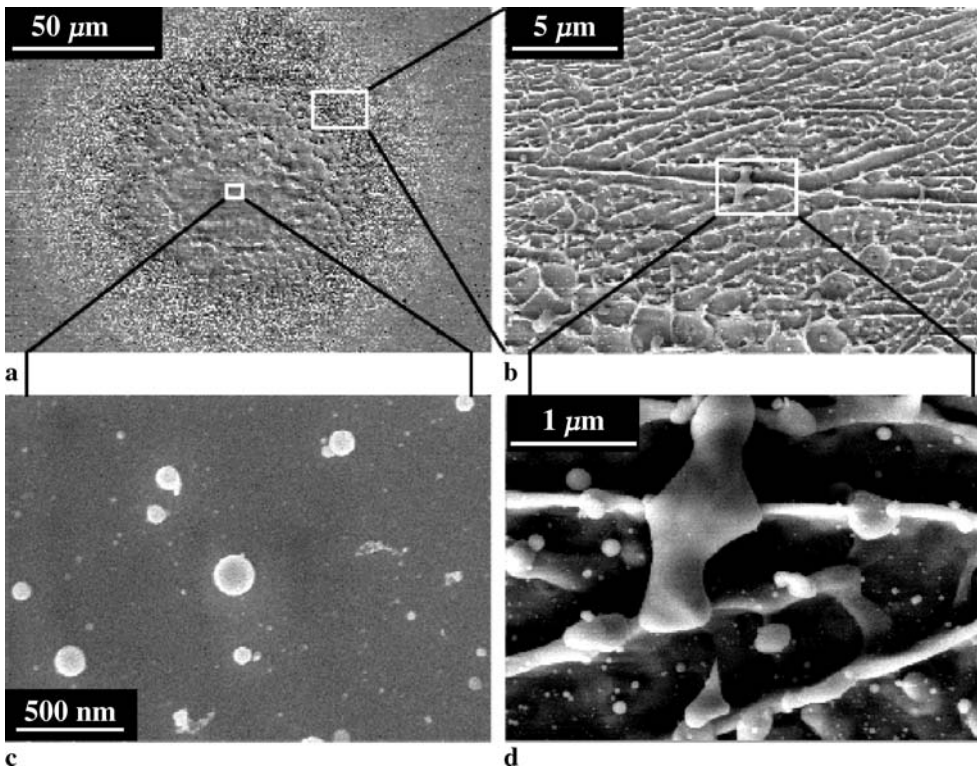

FIGURE 3   SEM images of the surface morphology of the irradiated spot after one-shot ablation of platinum at $F = 9.0\,\mathrm{J/cm^2}$ in 1-atm air: (**a**) the general view of the ablated spot; (**b**) micro- and nanostructural features on the periphery of the ablated spot; (**c**) spherical nanoparticles re-deposited in the central area of the ablated spot; (**d**) magnified view of the peripheral surface structures shown in (**b**). The diameter of the irradiated spot is about $100\,\mu\mathrm{m}$
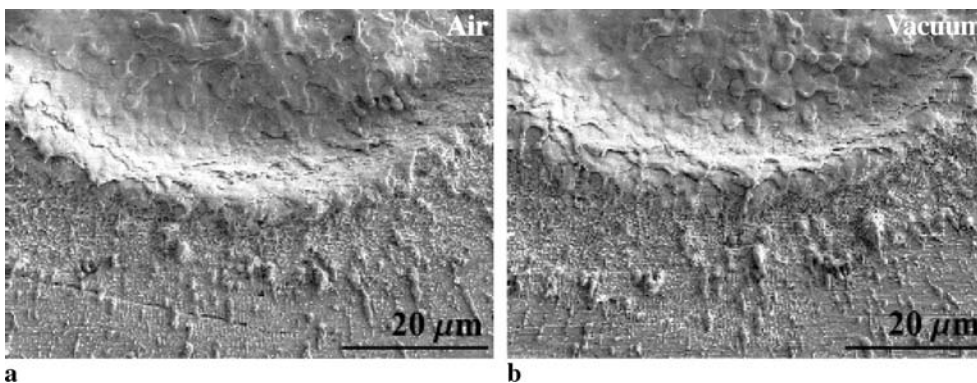

FIGURE 4   SEM images showing the onset of the cavity formation following 20-shot ablation at $F = 9.0\,\mathrm{J/cm^2}$ in air (**a**) and in vacuum (**b**)
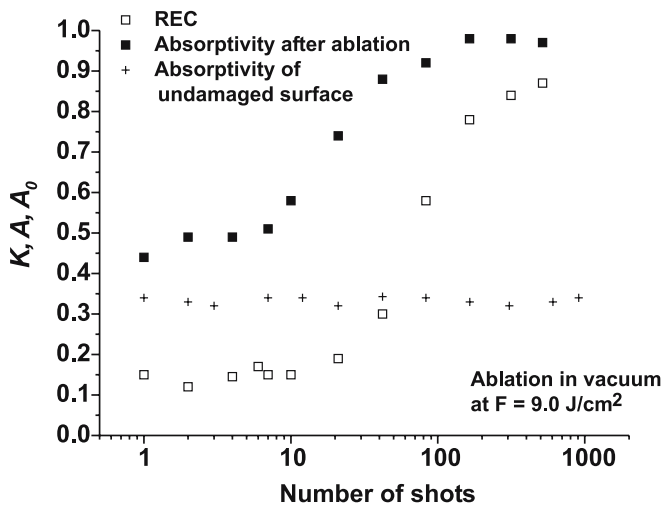
FIGURE 5 The pulse number dependences of residual energy coefficient and absorptance following ablation at $F = 9.0 \, \text{J/cm}^2$ in a vacuum at a base pressure of 6×10^{-3} Torr

contrasts with a much higher REC value we observe in air ($K = 0.76$, higher than the absorptance value). For N between 2 and about 20 shots, REC remains nearly constant at 0.15 despite the absorptance having increased from 0.44 to 0.74. For $N > 20$, REC increases significantly and reaches a value of about 0.85 at a large N. In the entire range of N, we notice that $K < A$ for ablation in vacuum, which contrasts with the relationship $K > A$ in air. We also took SEM images of surface morphology following ablation in vacuum under the same ablation conditions as in air and some representative images are shown in Fig. 6. A comparative analysis of the images taken for ablation in air versus in vacuum shows that the cen-

tral area of the ablated spot in vacuum is free of re-deposited nanoparticles (compare Fig. 6c with Fig. 3c) although a small amount of re-deposited particles may be observed on the peripheral area of the ablated spot. Figure 5 shows that both $K(N)$ and $A(N)$ begin to increase significantly for N in the range of 10–20 shots in vacuum. The SEM study reveals that these enhancements correlate with the cavity formation (see Fig. 4b). Therefore, for ablation both in air (Figs. 2 and 4a) and in vacuum (Figs. 5 and 4b), the onset of the significant REC and absorptance enhancements occurring at $N \approx 10$–30 corresponds to the formation of a crater.

To study the effects of laser fluence on REC and absorptance in multi-pulse ablation, we also measured $K(N)$ and $A(N)$ following ablation at a lower fluence of $3.6 \, \text{J/cm}^2$. The obtained results are plotted in Figs. 7. The comparison of these lower-fluence data with the higher-fluence data in Figs. 2 and 5 shows that the lower laser fluence mostly affects $K(N)$, and we observe the relationship $K < A$ at $F = 3.6 \, \text{J/cm}^2$ as opposed to $K > A$ at $F = 9.0 \, \text{J/cm}^2$. To further understand the effects of laser fluence on residual thermal coupling, we measured the fluence dependence of K following single-pulse ($N = 1$) ablation in air, neon, and vacuum by irradiating a fresh spot on the Pt sample after each shot. The behavior of $K(F)$ following a single femtosecond pulse ablation of an undamaged surface is shown in Fig. 9. We see that the three curves virtually overlap each other for $F < 1.2 \, \text{J/cm}^2$. However, these three curves start to branch out for $F > 1.2 \, \text{J/cm}^2$, i.e. REC increases both in air and in neon but decreases in vacuum. This measurement shows that the specific type of ambient gas plays very little role in affecting REC, but the presence of an ambient gas is the dominant factor for the enhanced REC. To further understand the ambient gas pressure effects on residual thermal energy deposition, we measured the pres-
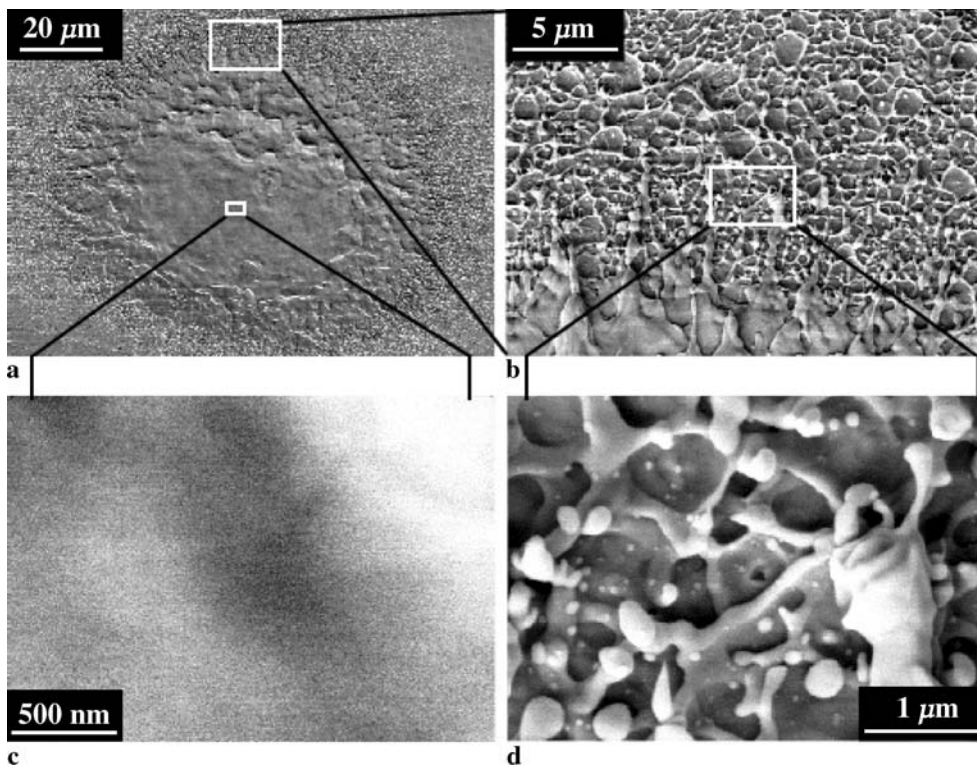

FIGURE 6 SEM images of surface morphology of the irradiated spot after one-shot ablation of platinum at $F = 9.0 \, \text{J/cm}^2$ in vacuum: (**a**) the general view of the ablated spot; (**b**) micro- and nanostructural features on the periphery of the ablated spot; (**c**) the magnified view of the central area of the ablated spot (there is no re-deposited nanoparticle as compared to Fig. 3c); (**d**) the magnified view of the peripheral surface structures shown in (**b**). The diameter of the irradiated spot is 100 μm
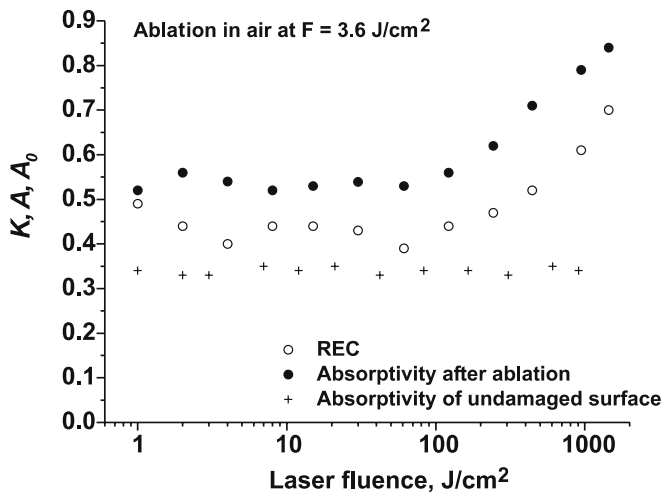
FIGURE 7   The pulse number dependences of residual energy coefficient and absorptance following ablation at $F = 3.6\,\mathrm{J/cm^2}$ in 1-atm air
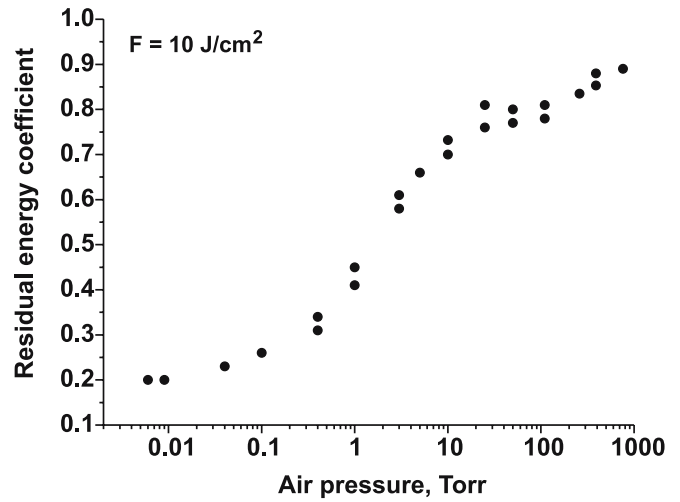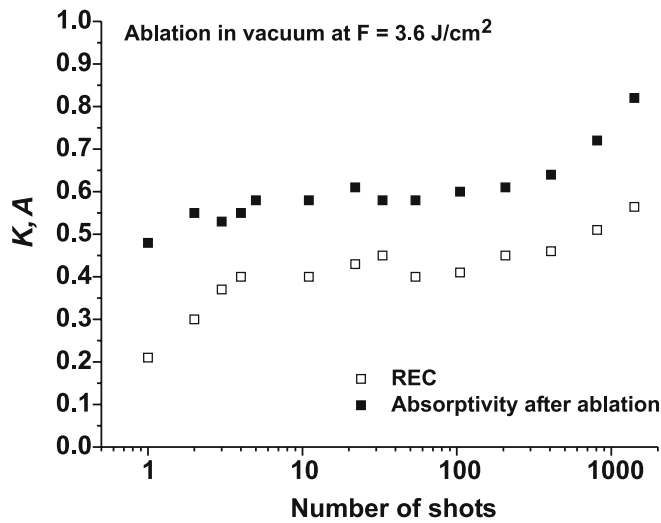

FIGURE 8   The pulse number dependences of residual energy coefficient and absorptance following ablation at $F = 3.6\,\mathrm{J/cm^2}$ in a vacuum at a base pressure of 6×10^{-3} Torr
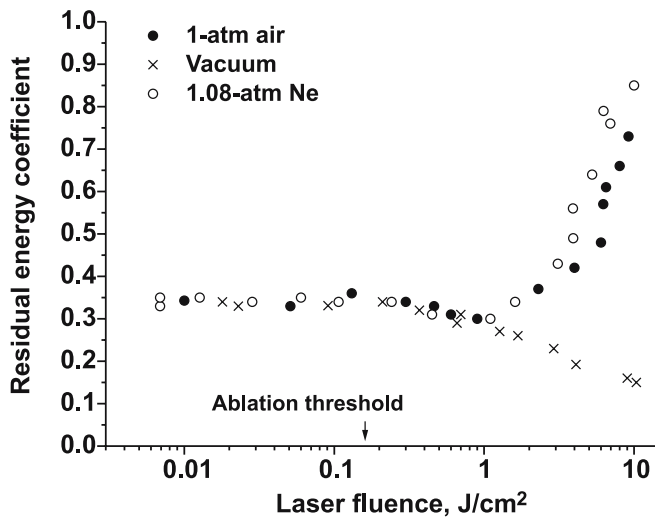

FIGURE 9   Residual energy coefficient for platinum as a function of laser fluence in 1-atm air, 1.08-atm Ne, and a vacuum at a base pressure of 6×10^{-3} Torr

FIGURE 10   Residual energy coefficient for platinum as a function of air pressure at $F = 10\,\mathrm{J/cm^2}$

sure dependence of K and the data are shown in Fig. 10. We can see that REC decreases as the ambient air pressure is lowered. This pressure dependence becomes insignificant in the low-pressure range, i.e. $P < 0.03$ Torr.

4   Discussion

Thermal response of metals following high-fluence laser irradiation has been studied in the past using microsecond [14] and nanosecond [15] laser pulses, and enhanced heat deposition in metals has been found in those experiments when plasmas are generated. To explain that enhanced thermal energy coupling, it has been suggested that energy transferring to a metal sample from laser-induced plasmas plays a key role [14]. Previously, we have found that the behavior of residual thermal energy coupling shows a similar general trend between nanosecond- and femtosecond-laser pulse ablation [9], and this suggests that the physical mechanism used to explain the long-pulse REC enhancement may also account for the behaviors of residual heating in femtosecond laser ablation. In general, two types of plasmas can be produced during a femtosecond laser pulse: (1) solid-density plasma in the skin layer of the sample and (2) ambient gas plasma. Solid-density plasma can be produced in both air and vacuum; in our experiment, however, the enhanced thermal coupling occurs only in air and, therefore, we believe that the solid-density plasma does not play a key role in the enhanced energy coupling. Therefore, we will subsequently focus our discussion on the effects of ambient air plasma.

The experimental data shown in Fig. 2 are obtained with an intensity of about $10^{14}\,\mathrm{W/cm^2}$. At this high intensity, direct ionization of the ambient air during the femtosecond laser pulse easily occurs by means of multi-photon and tunneling ionization even without the presence of a metal sample [16]. In the presence of a metal surface, the threshold of air ionization in front of the metal surface can be significantly reduced due to: (1) air exposed to the additional laser light reflected from the metal surface besides the incident light, (2) energetic electrons escaping from the metal surface due to multi-photon
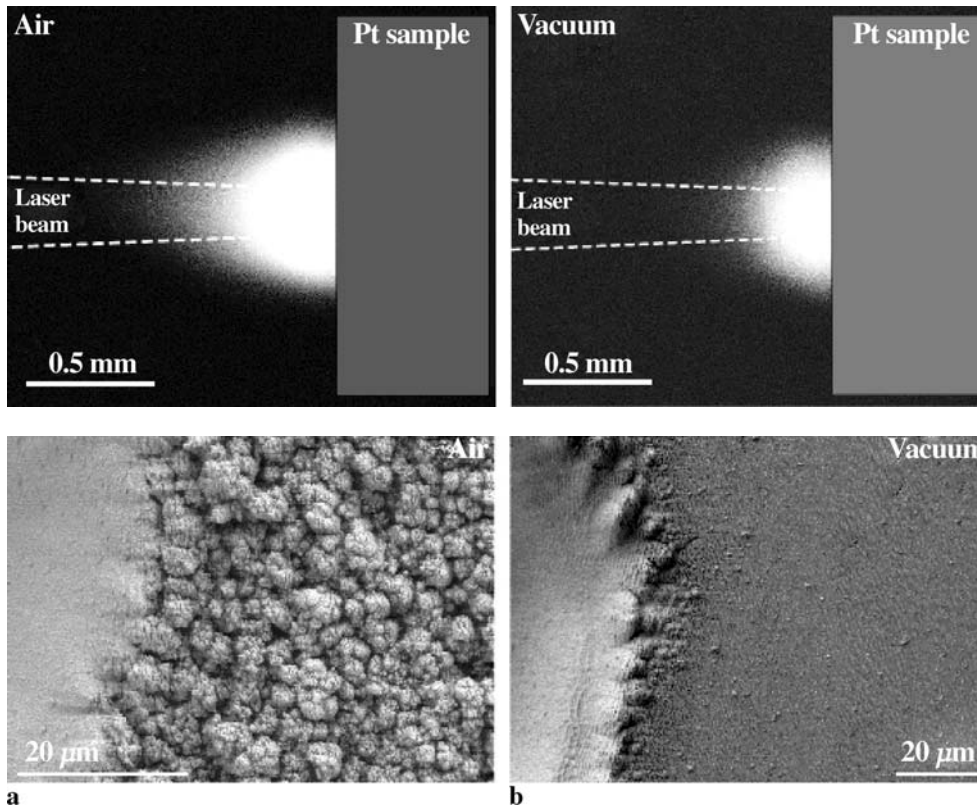
FIGURE 11 Open-shutter photographs of the plasma generated by single-pulse ablation at $F = 3.3 \, \text{J/cm}^2$ in 1-atm air and in vacuum ($P = 7 \times 10^{-3}$ Torr). The laser beam is incident normally onto the sample from the *left*

FIGURE 12 SEM images of the re-deposited materials on a platinum sample following 1500-pulse ablation at $F = 3.3 \, \text{J/cm}^2$ in (**a**) air and (**b**) vacuum. There is clearly more material re-deposition around the crater in air than in vacuum

photoelectron and thermionic emission [17], and (3) UV radiation from laser-induced solid-density plasma, if any. The above three processes will contribute additional air ionization besides the direct ionization from the incident light alone. It should be emphasized that this air plasma is produced prior to the hydrodynamic motion of the ablated material from the sample that occurs on the nanosecond time scale [18, 19]. We note that the generation of air plasma prior to the hydrodynamic motion of the ablated material has been observed in the past in picosecond laser ablation [20]. The difference between plasmas produced in air and in vacuum can clearly be seen from the plasma plume images in Fig. 11, which are taken using an open-shutter camera with a blue filter [9]. We can see that the size of hot plasma generated following ablation in air is larger than that in vacuum. Since material ejection in vacuum is not constrained by ambient gas, plumes formed in vacuum should have a larger size than that in air if they are formed only by the ejected metal particles. The fact that we see a larger plume size in air rather than in vacuum indicates that there must be air plasma generated by a high-intensity laser pulse. The formation of air plasma during a femtosecond pulse can enhance thermal energy coupling to a sample due to the following two pathways: (1) transferring the energy stored in the air plasma to the sample and (2) enhanced re-deposition of the ablated material back onto the sample due to the presence of a high pressure on the sample surface from the ambient gas plasma long after the femtosecond laser pulse. The decay time of the air plasma pressure, τ, is given by [21] $\tau = r/a_\text{p}$, where r is the radius of the irradiated spot and a_p is the sound speed in the plasma. For our ablation experiment in air, we estimate τ to be about 10 ns with $r = 50 \, \mu\text{m}$ and $a_\text{p} = 5 \, \text{km/s}$ [21]. In our experi-

ment, we observe a greater amount of particle re-deposition within the ablation spot in air following a single-pulse ablation; see e.g. SEM images in Figs. 3c and 6c. From the SEM images in Fig. 12, we again see a greater amount of material re-deposition around the crater in air compared to that in vacuum following multi-pulse ablation. Therefore, an enhanced re-deposition of the ablated materials in air following both single-pulse and multi-pulse ablation is confirmed experimentally.

By taking into account the above-mentioned enhanced thermal coupling assisted by air plasma, the behavior of REC in Fig. 2 can be explained as follows. For low N ($N < 12$) where REC decreases from 0.76 after the first pulse to 0.65 after 12 pulses, laser ablation mainly produces surface roughness (Fig. 3) and no crater is formed. This surface roughness will diffuse the surface backscattering, reduce the amount of reflected light absorbed by air plasma, and subsequently reduce the air-plasma-assisted heating of the sample. For $N > 12$, a cavity starts to develop (Fig. 4a), and this causes REC to increase with N. The cavity effects on the enhanced REC can be more clearly seen from the REC data in vacuum (Fig. 5) where the air-plasma effects are excluded: we can see from the figure that, for $N < 10$, REC is very low ($K \sim 0.15$) in vacuum without the contribution of air plasma, but increases significantly with N for $N > 10$ when a cavity is formed (Fig. 4b).

5   Conclusions

In this paper, we performed a shot-to-shot detailed study of how residual thermal energy depends on the absorptance change due to laser-induced surface structural modifications. Surprisingly, our study shows that, with a small number

of applied pulses in air, the enhanced residual thermal coupling following the first pulse ablation decreases with pulse number despite an enhanced absorptance. Both residual thermal coupling and absorptance increase with pulse number following a large number of applied pulses. To explain our observation at a low pulse number, we proposed a plasma-assisted mechanism for femtosecond laser ablation in a gas medium. Supported by our experimental results, we believe that the formation of ambient gas plasma enhances thermal energy coupling to a sample due to the following two pathways: energy transfer from the air plasma to the sample and enhanced re-deposition of hot ablated particles back onto the sample due to the presence of high pressure from the ambient gas plasma. These plasma-assisted effects can only play a role in a gas medium and are most important following a relatively low number of applied shots when only surface roughness but not a crater develops. At a large number of applied pulses, the residual heating of the sample is mainly governed by the formation of a cavity that enhances thermal energy coupling to the sample both in air and in vacuum. Although further studies are needed to better understand the physical mechanisms of thermal energy coupling to solids, our study provides new guidelines to determine the optimal thermal-loading conditions for achieving high-quality material processing using femtosecond laser pulses.

REFERENCES

1 S.I. Anisimov, B.S. Luk'yanchuk, Phys. Uspekhi **45**, 293 (2002)
2 S. Amoruso, G. Ausanio, R. Bruzzese, M. Vitello, X. Wang, Phys. Rev. B **71**, 033 406 (2005)
3 S. Nolte, B.N. Chichkov, H. Welling, Y. Shani, K. Liebermann, H. Terkel, Opt. Lett. **24**, 914 (1999)
4 J. Koch, F. Korte, T. Bauer, C. Fallnich, A. Ostendorf, B.N. Chichkov, Appl. Phys. A **81**, 325 (2005)
5 A.Y. Vorobyev, C. Guo, Opt. Express **14**, 2164 (2006)
6 P.P. Pronko, S.K. Dutta, J. Squier, J.V. Rudd, D. Du, G. Mourou, Opt. Commun. **114**, 106 (1995)
7 B.N. Chichkov, C. Momma, S. Nolte, F. von Alvensleben, A. Tunnermann, Appl. Phys. A **63**, 109 (1996)
8 G. Ausano, A.C. Barone, V. Iannotti, L. Lanotte, S. Amoruso, R. Bruzzese, M. Vitiello, Appl. Phys. Lett. **85**, 4103 (2004)
9 A.Y. Vorobyev, V.M. Kuzmichev, N.G. Kokody, P. Kohns, J. Dai, C. Guo, Appl. Phys. A **82**, 357 (2006)
10 A.Y. Vorobyev, C. Guo, Appl. Phys. Lett. **86**, 011 916 (2005)
11 A.Y. Vorobyev, C. Guo, Phys. Rev. B **72**, 195 422 (2005)
12 G.W.C. Kaye, T.H. Laby, *Tables of Physical and Chemical Constants*, 11th edn. (Longmans, London, 1956)
13 C. Wu, C.H. Crouch, L. Zhao, J.E. Carey, R. Younkin, J.A. Levinson, E. Mazur, R.M. Farrell, P. Gothoskar, A. Karger, Appl. Phys. Lett. **78**, 1850 (2001)
14 J.A. McKay, R.D. Bleach, D.J. Nagel, J.T. Schriemph, R.B. Hall, C.R. Pond, S.K. Manlief, J. Appl. Phys. **50**, 3231 (1979)
15 A.Y. Vorobyev, Sov. J. Quantum Electron. **15**, 490 (1985)
16 H.M. Milchberg, T.R. Clark, C.G. Durfee, T.M. Antonsen, P. Mora, Phys. Plasmas **3**, 2149 (1996)
17 J.G. Fujimoto, J.M. Liu, E.P. Ippen, Phys. Rev. Lett. **53**, 1837 (1984)
18 J. König, S. Nolte, A. Tünnermann, Opt. Express **13**, 10 597 (2005)
19 D. Breitling, A. Ruf, P.W. Berger, F.H. Dausinger, S.M. Klimentov, P.A. Pivovarov, T.V. Kononenko, V.I. Konov, Proc. SPIE **5121**, 24 (2003)
20 S.S. Mao, X. Mao, R. Greif, R.E. Russo, Appl. Phys. Lett. **76**, 31 (2000)
21 J.A. McKay, J.T. Schriemph, T.L. Cronburg, J.E. Eninger, J.A. Woodroffe, Appl. Phys. Lett. **36**, 125 (1980)